nature communications

Article

https://doi.org/10.1038/s41467-024-52200-0

Transient overturning changes cause an upper-ocean nutrient decline in a warming climate

Received: 12 April 2024

Accepted: 29 August 2024

Published online: 04 September 2024

Check for updates

Shantong Sun [1,2,3] ✉, Andrew F. Thompson [3], Jimin Yu [1,4,5] & Lixin Wu [1,6]

Models and proxy data suggest multi-centennial nutrient reorganization and biological productivity changes under sustained climate warming. These changes have traditionally been attributed to processes in the Southern Ocean. Here we instead show that transient overturning circulation adjustments, associated with changes in the Atlantic Meridional Overturning Circulation (AMOC), dominate the global nutrient reorganization on centennial timescales. Following an AMOC weakening, a typical feature of a warming climate, a transient overturning circulation develops in the Indo-Pacific basins, characterized by enhanced southward transport in the deep ocean. Coupled with the vertical nutrient structure, these transient overturning changes produce a net transport of nutrients from the Indo-Pacific into the Southern Ocean. Meanwhile, isopycnal surfaces deepen and bring nutrient-depleted waters to greater depths, causing nutrient concentrations to decline in much of the global upper ocean. Given the close link between nutrients and carbon, our findings suggest that transient overturning circulation changes across different basins can critically affect the marine carbon cycle.

Due to rising atmospheric CO_2, the ocean is experiencing changes in physical, chemical, and biological environments with critical impacts on ocean ecosystems[1–3]. Increases in surface stratification due to global warming are projected to limit surface nutrient supply and decrease biological productivity in low-to-mid latitudes during the 21st century. A global decline in biological productivity is likely to continue beyond the 21st century, but attributing this long-term change to enhanced surface stratification alone is difficult, because upper ocean changes occur on relatively short timescales[4,5]. Instead, long-term productivity changes are more likely caused by nutrient redistribution between different ocean basins and/or different water depths[2,6], with nutrient concentrations decreasing in much of the upper Atlantic and Indo-Pacific basins but increasing in the Southern Ocean. The associated mechanisms for this nutrient redistribution remain debated.

A recent study attributes global nutrient redistribution on centennial timescales to nutrient trapping in the Southern Ocean[2], hinging on coupled changes in wind-driven deep water upwelling and biological activity in the Southern Ocean. As the climate warms, Southern Hemisphere westerly winds are predicted to shift poleward and intensify[7,8], potentially increasing circumpolar upwelling of nutrient-rich deep waters in the Southern Ocean. The resulting biological productivity enhancement in the Southern Ocean, due to nutrient increases and favorable warm growth conditions, would increase the vertical export of organic matter that transfers nutrients from the surface to the deep ocean, where sinking particles are remineralized. This enhanced biological export reduces nutrient concentrations in the northward subducting waters that sustain low-latitude biological productivity today[9]. Together, these processes are thought to result in nutrient trapping in the Southern Ocean[2]. Critically, if these Southern

[1]Laoshan Laboratory, Qingdao, China. [2]Earth, Ocean and Atmospheric Science, Florida State University, Tallahassee, FL, USA. [3]Environmental Science and Engineering, California Institute of Technology, Pasadena, CA, USA. [4]Research School of Earth Sciences, Australian National University, Canberra, ACT, Australia. [5]SKLLQG, Institute of Earth Environment, Chinese Academy of Sciences, Xi'an, China. [6]Frontiers Science Center for Deep Ocean Multispheres and Earth System/Key Laboratory of Physical Oceanography, Ocean University of China, Qingdao, China. ✉e-mail: stsun@qnlm.ac

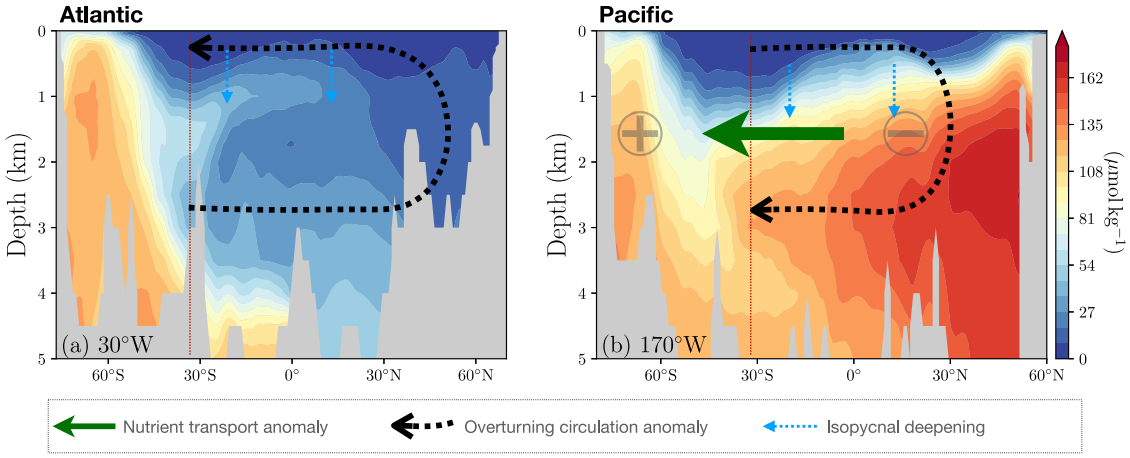

Fig. 1 | Schematic showing tracer redistributions by transient ocean overturning changes. Color shadings show climatological distributions of dissolved inorganic silicate (Si) from GLODAPv2[52] along **a** 30° W in the Atlantic and **b** 170° W in the Pacific. Following a slowdown of the Atlantic overturning (black dashed line with arrow in (**a**) shows the overturning anomaly), the Indo-Pacific develops an opposite overturning circulation anomaly (black dashed line with arrow in (**b**)). These transient overturning circulation changes redistribute Si between the Southern Ocean and the northern basins, which increases Si in the Southern Ocean ("+") and reduces Si in the Indo-Pacific ("−"). Associated with these overturning adjustments, isopycnal surfaces deepen (blue dashed arrows) and bring nutrient-depleted surface waters to greater depths, decreasing nutrient concentrations in the upper Atlantic and Indo-Pacific. The red dotted lines represent the boundary between the Southern Ocean and the northern basins.

Ocean processes dominate the centennial global nutrient redistribution, the upper-ocean nutrient reduction would be most prominent in the Southern Hemisphere, due to the northward subducting intermediate and mode waters. However, this cannot fully explain the nutrient structure changes simulated by earth system models[2], where nutrient concentrations decline more significantly in the Northern Hemisphere. Thus, additional processes are required to explain Southern Ocean nutrient trapping and global nutrient redistribution.

Investigation of nutrient cycling in the ocean is also important for understanding past ocean and climate changes. Multi-centennial nutrient reorganization occurred during the last deglaciation. Paleoclimate records suggest enhanced diatom production around the Antarctic Polar Front during Heinrich events[10,11], when the Atlantic Meridional Overturning Circulation (AMOC) was believed to be substantially weakened[12,13]. The enhanced diatom production was interpreted as evidence for increased Southern Ocean upwelling of nutrient-rich deep waters[10,11,14], driven by an intensification and/or southward shift of Southern Hemisphere westerly winds[15,16]. However, more recent theoretical and modeling studies suggest a much weaker sensitivity of the Southern Ocean upwelling to westerly wind changes due to compensation effects from transient and standing eddies[17–20]. Thus, the dominant factors affecting the centennial global nutrient redistribution warrant further investigation.

In this study, we highlight the role of transient overturning circulation responses, involving interactions between the Atlantic and the Indo-Pacific basins, in the global redistribution of nutrients and biological productivity reduction in a warming climate on centennial time scales (Fig. 1). Following a weakening of the AMOC, a typical feature of a warming climate[21,22], the Indo-Pacific ocean develops an overturning circulation anomaly that opposes the Atlantic changes (black dashed arrows in Fig. 1)[23]. This inter-ocean response is established via the propagation of planetary waves, associated with a global adiabatic deepening of density surfaces (blue dashed arrows in Fig. 1)[23–25]. This process is distinct from previous views of Indo-Pacific overturning changes that involve the initiation/enhancement of deep and/or intermediate water formation in the Pacific[26–29].

More specifically, changes in the AMOC modify the density structure in the North Atlantic. The associated stratification changes propagate into the South Atlantic and the Indo-Pacific, leading to geostrophically-balanced, meridional volume transport anomalies that have opposing signs between the Atlantic and Indo-Pacific basins (dashed arrows in Fig. 1). This process affects the global distribution of heat[25] and biogeochemical tracers, but has been underappreciated and underexplored in previous studies. Coupled with the vertical structure of nutrient concentrations, the transient overturning response in the Indo-Pacific causes a global reorganization of nutrients between different ocean basins (green arrow in Fig. 1), affecting global biological productivity in a warming climate.

Results

Nutrient and productivity changes in a warming climate

We use outputs from the Community Earth System Model 2 (CESM2; see "CESM2 simulations" in "Methods"), as part of the Coupled Model Intercomparison Project Phase 6[30]. In response to atmospheric CO_2 quadrupling ("4×CO_2"), the surface ocean stratification increases rapidly over the first 100 years, due to surface warming, and then levels off (Supplementary Fig. 1). This rapid stratification increase, which restricts nutrient entrainment into the euphotic layer ("CESM2 simulations" in "Methods"), suppresses diatom production and organic matter export in the Atlantic and Indo-Pacific basins (Supplementary Figs. 2 and 3).

Primary production continues to decrease in much of the Indo-Pacific and Atlantic basins over the next few centuries (Fig. 2a, b and Supplementary Fig. 2). However, these long-term biogeochemical responses can no longer be explained by surface stratification, which only increases minimally after ~100 years. Instead, the multi-centennial decline in biological production is related to a global reorganization of nutrients (Fig. 2c–f and Supplementary Figs. 4 and 5). Here we focus on the distribution of dissolved inorganic silicate (Si), which is critical to diatom production and surface organic matter export[31]. Si decreases in much of the subsurface Indo-Pacific basin, with maximum reductions at around 1 km water depth in the North Pacific, and in the upper 1.5 km of the Atlantic, but Si increases in much of the Southern Ocean and in the deep Atlantic, exhibiting a nutrient redistribution between different ocean basins (Fig. 2).

This nutrient redistribution was previously attributed to wind-driven circumpolar enhancement of deep water upwelling and increases in biological production in the Southern Ocean[2], but this mechanism cannot fully explain the structure of nutrient changes in the Pacific Ocean. Specifically, if the global nutrient redistribution is dominated by Southern Ocean processes, the enhanced biological

https://doi.org/10.1038/s41467-024-52200-0

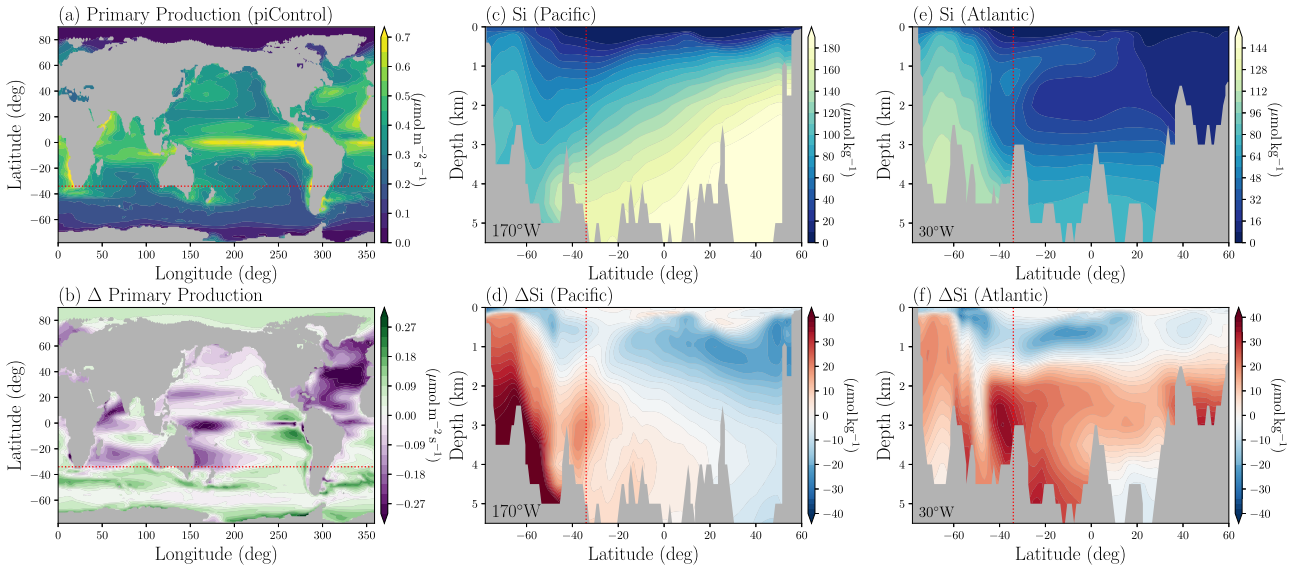

Fig. 2 | Nutrients and primary production in CESM2. a Primary production in the pre-industrial Control run (piControl), averaged over the last 50 years. **b** Primary production changes after CO_2 quadrupling, averaged over years 150–200. **c** Si concentration along 170° W in the Pacific. **d** Si concentration changes (ΔSi) after CO_2 quadrupling, averaged over years 150–200. **e** Same as (**c**) but along 30° W in the Atlantic. **f** Same as (**d**) but along 30° W in the Atlantic. The red dotted lines represent the boundary between the Southern Ocean and the northern basins. Source data are provided as a Source Data file.

production would lead to the largest nutrient reductions in the cores of intermediate/mode waters in the Southern Hemisphere near 1 km water depth, inconsistent with the simulated substantial nutrient reductions in the North Pacific (Fig. 2d). We note that a long-term decline of biological productivity in the northern basins may reduce subsurface nutrient levels in the North Pacific, but the associated processes would primarily redistribute nutrients vertically along the water column, not between ocean basins (Supplementary Fig. 5).

Transient overturning circulation adjustments and nutrient redistribution

The global nutrient redistribution, occurring on centennial timescales, is better explained by transient adjustments of the global ocean overturning circulation. Following atmospheric CO_2 quadrupling, the ocean's overturning circulation adjusts to changes in surface forcing. A prominent feature is a slow-down of the AMOC (Fig. 3a and Supplementary Fig. 6)[22]. At similar water depths where the AMOC weakens, an overturning circulation anomaly with an opposing sign develops in the Indo-Pacific (Fig. 3a, b), characterized by a northward transport anomaly in the upper 1 km and a southward transport anomaly at greater depths (dashed arrow in Fig. 1b). During the overturning circulation adjustments, the Indo-Pacific overturning response, $\Delta\psi_P$, largely compensates for the AMOC weakening, $\Delta\psi_A$, at 30° S on centennial timescales, i.e., $\Delta\psi_P \approx -\psi_A$ (Supplementary Fig. 6b). However, nutrient distributions differ between the Atlantic and Indo-Pacific. Nutrients are more enriched in the deep Indo-Pacific and have stronger vertical gradients over the upper 3 km due to weaker ventilation, as compared to the Atlantic (Figs. 1 and 2c, e). As such, when the compensating overturning circulation changes in the Indo-Pacific and the Atlantic basins are coupled with the different vertical nutrient gradients, a net redistribution of nutrients into the Southern Ocean occurs (see "Nutrient transport" in "Methods").

To demonstrate the above mechanism, we quantify the Si transport anomalies, $\Delta\mathcal{T}$, between the Southern Ocean and the northern basins across 30° S in the model (see "Nutrient transport" in "Methods"). We find a southward Si transport anomaly, $\Delta\mathcal{T} < 0$, into the Southern Ocean (purple line in Fig. 3d), which is driven by circulation changes (Supplementary Fig. 7) and dominates over changes in diffusive nutrient transport (Supplementary Fig. 8). The southward Si redistribution causes nutrient trapping in the Southern Ocean with the Southern Ocean Si content increasing by 37% in 1,000 years (Supplementary Fig. 8). A further decomposition of the Si transport into different basins shows that the Southern Ocean Si increase arises from exchanges with the Indo-Pacific basin (red line in Fig. 3c), and thus, is not a circumpolar response as suggested in previous studies. The associated southward Si transport anomaly is due to transient overturning circulation responses, linked to the concomitant AMOC weakening, coupled to characteristic Si distributions with enriched Si and stronger vertical gradient in the Indo-Pacific (orange line in Fig. 3c). The Si transport is northward across 30° S in the Atlantic basin (blue line in Fig. 3c), largely due to the AMOC weakening (green line in Fig. 3c). Taken together, we show that transient overturning circulation changes can substantially impact large-scale nutrient transport and redistribution in the world oceans (Fig. 3).

We reach the same conclusion using previous model outputs[2], i.e., the centennial nutrient redistribution between the Southern Ocean and the northern basins in a warming climate is predominantly due to transient overturning circulation adjustments between the Indo-Pacific and the Atlantic (Supplementary Fig. 9). While the previously proposed mechanism for Southern Ocean nutrient trapping may be useful to explain intermediate depth nutrient changes, we continue to find that overturning circulation changes and the associated isopycnal deepening are necessary to account for most of the nutrient changes in the subsurface Indo-Pacific and the upper Atlantic oceans (see "Nutrient changes due to adiabatic isopycnal movements" in "Methods"; Supplementary Fig. 10). Specifically, isopycnal surfaces deepen to balance the transient overturning adjustment[23] and bring nutrient-depleted water to greater depths (blue arrows in Fig. 1), causing nutrient concentrations to decline in much of the global upper ocean.

Roles of wind and buoyancy

The poleward shift and strengthening of Southern Hemisphere westerly winds (Supplementary Fig. 11) has been thought to cause stronger upwelling of nutrient-rich deep waters[15,32] and also contribute to nutrient increases in the Southern Ocean. However, in the CESM2 simulations, the Southern Ocean overturning circulation changes only briefly produce a small southward Si transport anomaly during the first 100 years, and then the sign reverses (pink line in Fig. 3d). Thus, the nutrient

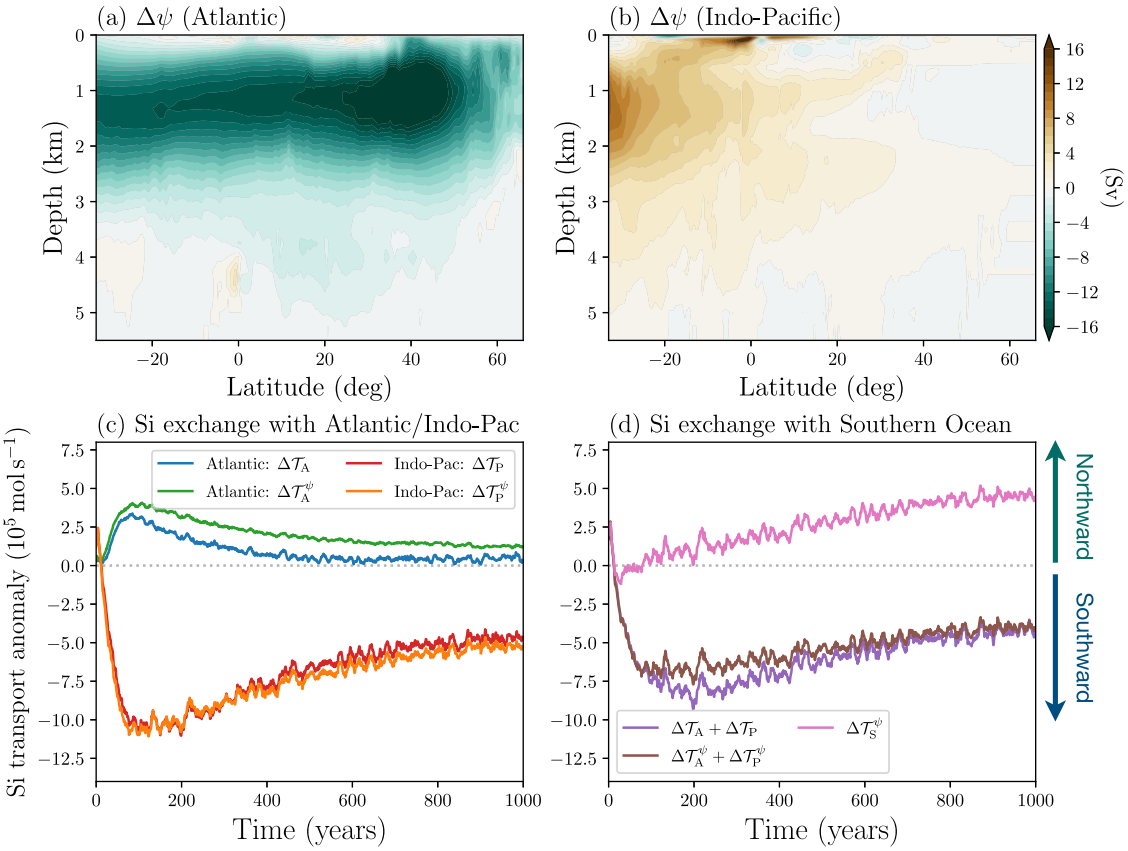

Fig. 3 | Overturning responses and nutrient redistribution in CESM2 4×CO_2 experiment. a Changes in the AMOC stream function after CO_2 quadrupling (negative for anticlockwise), averaged over years 150–200. **b** Same as (**a**) but for the Indo-Pacific overturning. **c** Si transport anomalies ($\Delta\mathcal{T}_A$, $\Delta\mathcal{T}_P$) and their contributions due to overturning circulation changes ($\Delta\mathcal{T}_A^\psi$, $\Delta\mathcal{T}_P^\psi$) across the southern boundary (30° S) of the Atlantic (subscript "A") and Indo-Pacific basins (subscript "P"). **d** Same as (**c**) but for the net Si transport anomaly between the Southern Ocean and the northern basins. The Si transport anomaly due to Southern Ocean overturning changes, $\Delta\mathcal{T}_S^\psi$, is plotted as a pink curve. Negative values in (**c** and **d**) represent southward transport anomalies. Source data are provided as a Source Data file.

redistribution into the Southern Ocean is unlikely due to surface wind induced circumpolar upwelling changes[2]. To explore the underlying processes that affect the overturning circulation and nutrient redistribution, we assess the respective roles of surface winds and buoyancy changes, which have been extensively studied but heavily debated in the literature.

We use an ocean-biogeochemical model, based on MITgcm, to carry out a set of process-based numerical experiments, which allow us to separate the respective roles of wind and buoyancy in affecting the overturning circulation and nutrient redistribution (see "Ocean-biogeochemical model setup" in "Methods"). Under surface wind and buoyancy forcings from CESM2 4×CO_2, our MITgcm runs largely reproduce the global ocean nutrient reorganization in CESM2 (Supplementary Fig. 12). Most of the global nutrient redistribution is attributable to changes in surface buoyancy forcing, rather than surface winds (Fig. 4 and Supplementary Fig. 13). The strengthening and poleward shift of Southern Hemisphere westerly winds increases Ekman pumping and surface nutrients only in regions close to Antarctica (Fig. 4a–c). In the broader Antarctic Circumpolar Current region, however, the southward shift of westerly winds weakens Ekman pumping and shifts the nutrient-rich deep waters to greater depths, leading to a decrease in surface nutrient concentrations (Supplementary Fig. 14; see "Nutrient changes due to adiabatic isopycnal movements" in "Methods"). Changes in surface buoyancy forcing, due to CO_2 quadrupling, cause a reduction in nutrient concentrations in much of the global upper 2 km (Fig. 4d–f) that resembles nutrient changes in CESM2 4×CO_2 (Fig. 2d, f), along with the southward nutrient redistribution driven by transient overturning changes (Supplementary Fig. 13c). Despite nutrient increases in the subsurface Southern Ocean, surface nutrient concentrations decline in the Southern Ocean. This likely occurs because surface warming and freshening increase surface stratification[33] and reduce nutrient supply into the surface mixed layer from the deep ocean.

The MITgcm results show that changes in Southern Hemisphere westerly winds only marginally affect the global nutrient distribution. Therefore, we conclude that changes in surface buoyancy cause transient adjustments of the global overturning circulation that redistribute nutrients from the Indo-Pacific into the Southern Ocean.

Discussion

The deep Indo-Pacific contains a large amount of dissolved inorganic nutrients and carbon. Yet, previous studies on the ocean's role in climate transitions have largely focused on physical processes that connect the overturning circulation between the Atlantic and the Southern Ocean. The impact of Indo-Pacific overturning changes remains critically under-explored. A change in the strength and structure of the AMOC is likely to be a key component of the climate's response to anthropogenic forcing. Transient adjustments of the overturning circulation on centennial timescales associated with AMOC changes, as shown recently, involve interactions primarily between the Atlantic and the Indo-Pacific[23] and could affect distributions of biogeochemical tracers, including nutrients and carbon. Here, we show that transient Indo-Pacific overturning circulation changes, associated with AMOC weakening, cause a southward nutrient redistribution from the Indo-

https://doi.org/10.1038/s41467-024-52200-0

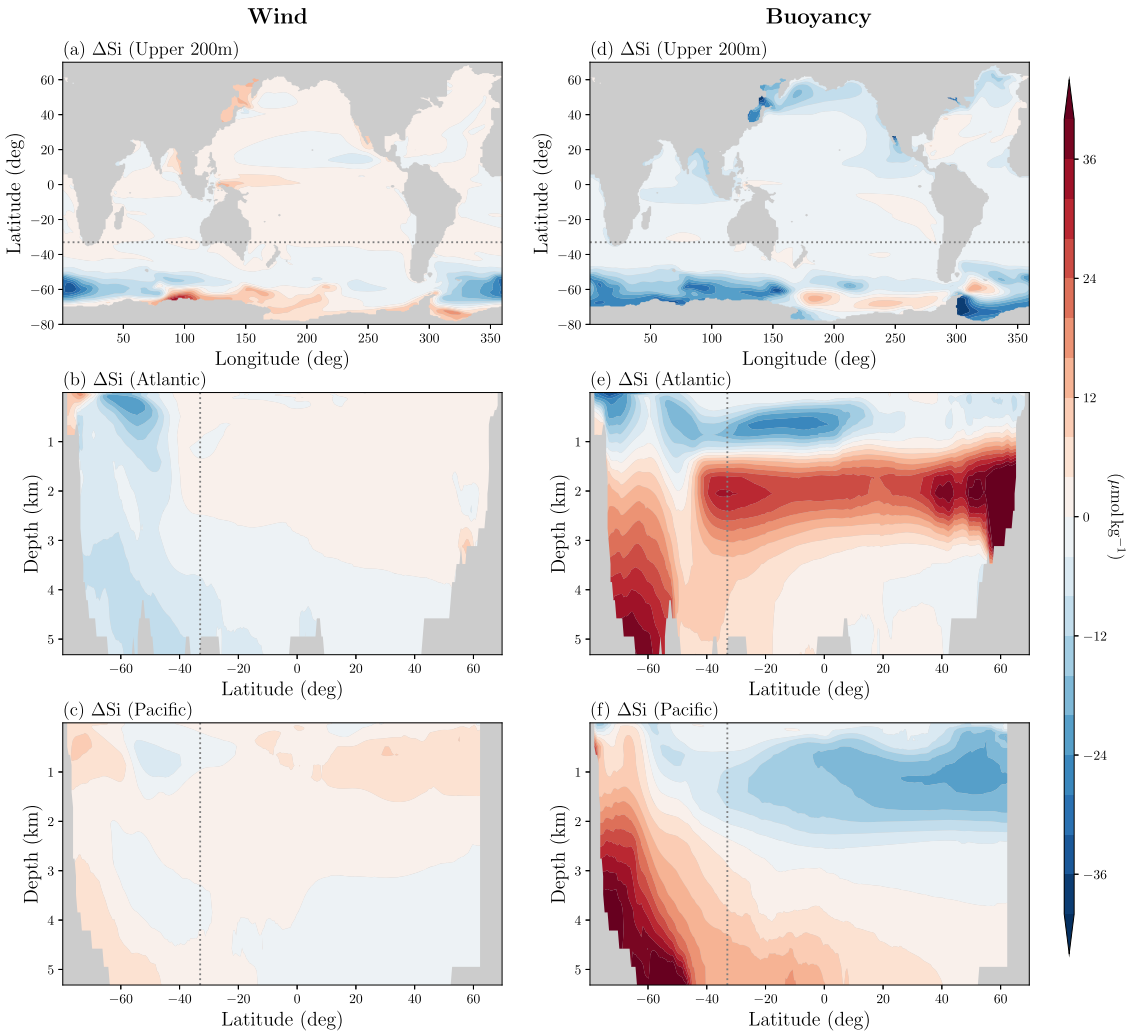

Fig. 4 | Si responses to surface forcing changes in the ocean-biogeochemical model, based on MITgcm. a–c Si changes, *Δ*Si, when forced with surface wind from CESM2 4×CO_2. **d–f** Si changes, *Δ*Si, when forced with surface buoyancy forcing from CESM2 4×CO_2. *Δ*Si values are (**a**, **d**) vertically averaged in the upper 200 m and **b**–**f** zonally averaged in the **b**, **e** Atlantic and **c**, **f** Indo-Pacific basins. *Δ*Si is calculated as the difference from the MITgcm control run, which is forced with surface forcing taken from CESM2 piControl. For modeling details, see "Ocean-biogeochemical model setup" in "Methods". Source data are provided as a Source Data file.

Pacific into the Southern Ocean in a warming climate and lead to nutrient trapping in the Southern Ocean. This nutrient reorganization contributes to a long-term decline of oceanic biological productivity in the Indo-Pacific, as documented previously[34–36].

The transient overturning circulation adjustments also provide mechanistic insights into past climate changes. For example, coral temperature records show significant subsurface warming in the eastern equatorial Pacific during Heinrich events and the Younger Dryas during the last deglaciation[37]. The subsurface warming on multi-centennial time scales is most likely due to isopycnal deepening in the broad low-to-mid latitudes that balances the Indo-Pacific overturning circulation anomalies associated with AMOC weakening[25]. The nutrient redistribution by transient overturning changes might have also supplied more Si to the Southern Ocean and contributed to increases in diatom production close to the Antarctic Polar Front during Heinrich events[10,14]. However, we note that diatom records during Heinrich stadials represent mean climate variations under different background climate conditions and on timescales (multi-centennial to millennial) longer than those discussed in this study. Further studies are required to understand processes controlling past ocean circulation, nutrient reorganizations, and the time scales over which these processes occur.

Nutrient cycling is intrinsically linked to the global ocean carbon cycle and atmospheric CO_2 changes. Previous studies have heavily relied on Southern Ocean processes (e.g., changes to westerly winds) to explain changes in nutrient distribution and carbon cycle[2,32,38]. Our study suggests that processes in the North Atlantic, via transient overturning circulation changes between the Atlantic and the Indo-Pacific basins, play a critical role in regulating global nutrient distributions on centennial timescales. The global upper-ocean nutrient decline (Fig. 2) due to transient overturning changes suggests a more efficient biological carbon pump that may help increase oceanic CO_2 uptake[39]. Dissolved inorganic carbon and Si have similar distributions in the ocean. Thus, transient overturning circulation adjustments, associated with AMOC changes, also inevitably redistribute carbon between different ocean basins and trap more carbon in the deep ocean as well as in the Southern Ocean (Supplementary Fig. 15), increasing deep ocean carbon storage.

Methods

CESM2 simulations

CESM2 is a fully coupled earth system model, consisting of ocean, atmosphere, land, sea ice, land ice, and wave components, which exchange states and fluxes through a coupler[40]. The ocean component

is Parallel Ocean Program version 2 and has a nominal horizontal resolution of 1°. Ocean biogeochemistry in CESM2 is represented by the Marine Biogeochemistry Library (MARBL), which represents multiple nutrient colimitations (N, P, Si, and Fe). MARBL includes fully prognostic carbonate chemistry and simulates sinking particulate organic matter implicitly. There are three explicit phytoplankton functional groups (diatoms, diazotrophs, and pico/nano phytoplankton), one implicit group (calcifiers), and one zooplankton group. The piControl run approximately simulates the observed structure of nutrients in the upper 3 km (Fig. 2), but overestimates the abyssal nutrients level due to the too-weak abyssal overturning circulation[41]. The CESM2 CO_2 quadrupling ($4\times CO_2$) experiment is initialized from piControl, but with the atmospheric CO_2 instantaneously quadrupled. The $4\times CO_2$ run is continued for another 1,000 years. Unless otherwise noted, we compare $4\times CO_2$ averaged over years 150–200 with piControl.

During the first few decades, the reduced nutrient entrainment into the surface due to stronger stratification leads to a slight increase in nutrient concentrations below the surface mixed layer (Supplementary Fig. 5). The surface nutrient depletion favors picophytoplankton, which are better adapted to the low-nutrient environment, and their production increases due to the favorable warm growth conditions during the first few decades (green lines in Supplementary Fig. 2b, c). The picophytoplankton increase overwhelms the diatom decrease in primary production in the short term but does not contribute substantially to organic matter export to the subsurface ocean (Supplementary Fig. 3).

Regional changes in primary production are not exclusively controlled by nutrient concentrations (Supplementary Fig. 4). In low-to-mid latitudes, where diatom growth is somewhat limited by Si availability, diatom production tends to decrease in regions where Si concentration declines. However, primary production and organic matter export increase in the Southern Ocean (Supplementary Figs. 2 and 3), a typical high-nutrient low-chlorophyll region[42], despite a decrease in surface Si concentration. This likely occurs due to a reduction in summer sea ice coverage close to Antarctica and surface warming in lower latitudes[43], which relieves light limitation.

Nutrient transport

We calculate the nutrient transport across 30° S, $\mathcal{T}$, as,

$$\mathcal{T} = \int_{z_{\mathrm{bot}}}^{0}\int_{x_w}^{x_e} v\mathcal{N}\, dx\, dz, \tag{1}$$

where $\mathcal{N}$ is nutrient concentration, v represents residual velocity, including the Eulerian-mean flow and eddies, x_w and x_e denote the western and eastern boundaries, respectively. Differences in nutrient transport between piControl and $4\times CO_2$, $\Delta\mathcal{T}$, can be driven by changes in ocean circulation, v', as well as changes in nutrient concentrations due to other processes, $\mathcal{N}'$,

$$\Delta\mathcal{T} = \int_{z_{\mathrm{bot}}}^{0}\int_{x_w}^{x_e} \left(v'\mathcal{N}_0 + v_0\mathcal{N}'\right) dx\, dz, \tag{2}$$

where $\mathcal{N}_0$ and v_0 represents nutrient concentration and velocity, respectively, in piControl, and we neglected contributions due to $v'\mathcal{N}'$. Our calculation suggests that circulation changes in $4\times CO_2$ relative to piControl,

$$\Delta\mathcal{T}^{v} \equiv \int_{z_{\mathrm{bot}}}^{0}\int_{x_w}^{x_e} v'\mathcal{N}_0 dx\, dz,$$

dominates the nutrient transport anomaly, $\Delta\mathcal{T}$ (Supplementary Fig. 7), i.e., $\Delta\mathcal{T}\approx\Delta\mathcal{T}^{v}$.

The nutrient transport changes due to circulation differences, $\Delta\mathcal{T}^{v}$, can be further decomposed into contributions due to changes in ocean overturning circulation, $\Delta\mathcal{T}^{\psi}$, and horizontal circulation (e.g., gyres), $\Delta\mathcal{T}^{\mathrm{G}}$,

$$\Delta\mathcal{T}^{v} = \int_{z_{\mathrm{bot}}}^{0}\int_{x_w}^{x_e} (\overline{v}+\hat{v})\mathcal{N}_0 dx\, dz = \underbrace{\int_{z_{\mathrm{bot}}}^{0} \Delta\psi \frac{\partial\overline{\mathcal{N}}_0}{\partial z} dz}_{\Delta\mathcal{T}^{\psi}} + \underbrace{\int_{z_{\mathrm{bot}}}^{0}\int_{x_w}^{x_e} \hat{v}'\hat{\mathcal{N}}_0 dx\, dz}_{\Delta\mathcal{T}^{G}}, \tag{3}$$

where overline means zonal average between x_w and x_e, hat means deviations from zonal average, and $\Delta\psi$ represents overturning circulation differences between piControl and $4\times CO_2$, defined as,

$$\Delta\psi(z) = \int_{z_{\mathrm{bot}}}^{z}\int_{x_w}^{x_e} \overline{v}' dx\, dz. \tag{4}$$

The nutrient exchange across 30° S, $\Delta\mathcal{T}$, occurs in both the Atlantic, $\Delta\mathcal{T}_{\mathrm{A}}$, and the Indo-Pacific sectors, $\mathcal{T}_{\mathrm{P}}$,

$$\Delta\mathcal{T} \equiv \Delta\mathcal{T}_{\mathrm{A}} + \mathcal{T}_{\mathrm{P}} \approx \Delta\mathcal{T}^{v}_{\mathrm{A}} + \Delta\mathcal{T}^{v}_{\mathrm{P}}.$$

Applying the decomposition in Eq. (3) for each basin, we have

$$\Delta\mathcal{T} \approx \underbrace{\Delta\mathcal{T}^{\psi}_{\mathrm{A}} + \mathcal{T}^{\psi}_{\mathrm{P}}}_{\Delta\mathcal{T}^{\psi}_{i}} + \Delta\mathcal{T}^{\mathrm{G}}_{\mathrm{A}} + \Delta\mathcal{T}^{\mathrm{G}}_{\mathrm{P}}, \tag{5}$$

where the nutrient transport anomaly due to the compensating overturning transient between the Atlantic and Indo-Pacific basins,

$$\Delta\mathcal{T}^{\psi}_{i} = \int_{z_{\mathrm{bot}}}^{0}\left(\Delta\psi_{\mathrm{P}}\frac{\partial\overline{\mathcal{N}}_{\mathrm{P}}}{\partial z} + \Delta\psi_{\mathrm{A}}\frac{\partial\overline{\mathcal{N}}_{\mathrm{A}}}{\partial z}\right)dz \approx \int_{z_{\mathrm{bot}}}^{0}\Delta\psi_{P}\left(\frac{\partial\overline{\mathcal{N}}_{\mathrm{P}}}{\partial z} - \frac{\partial\overline{\mathcal{N}}_{\mathrm{A}}}{\partial z}\right)dz < 0 \tag{6}$$

where $\overline{\mathcal{N}}_{\mathrm{A}}$ and $\overline{\mathcal{N}}_{\mathrm{P}}$ represent the zonal-mean nutrient concentration calculated in the Atlantic and the Indo-Pacific basin, respectively, in piControl. The Indo-Pacific overturning circulation anomaly at 30° S, $\Delta\psi_P$, is positive (Fig. 3b). The vertical nutrient gradient is much stronger in the Indo-Pacific basin, $\frac{\partial\overline{\mathcal{N}}_{\mathrm{P}}}{\partial z} - \frac{\partial\overline{\mathcal{N}}_{\mathrm{A}}}{\partial z} < 0$, due to the slower ventilation rate in the deep Pacific than in the deep Atlantic[44]. As such, the compensating overturning circulation transients drive a southward nutrient transport anomaly into the Southern Ocean.

Nutrient changes due to adiabatic isopycnal movements

The Indo-Pacific overturning responses in Fig. 3b are largely balanced by an adiabatic deepening of isopycnals. This process brings nutrient-depleted water to greater depth (Fig. 1) and contributes to the nutrient decrease in Fig. 2d. For conciseness, we consider a one-dimensional case. For piControl,

$$\mathcal{N} = N_0(z), z = \zeta_0(b), b = B_0(z), \tag{7}$$

and for $4\times CO_2$,

$$\mathcal{N} = N_1(z), z = \zeta_1(b), b = B_1(z), \tag{8}$$

where $\mathcal{N} = N(z)$ represents nutrient distribution as a function of depth, $z = \zeta(b)$ denotes the depth of isopycnal of buoyancy b, and $b = B(z)$ is the vertical buoyancy distribution. As such, the nutrient changes between piControl and $4\times CO_2$ due to adiabatic isopycnal movements can be quantified as

$$\Delta\mathcal{N}_h(z) = N_0\left(\zeta_0(B_1(z))\right) - N_0(z), \tag{9}$$

Changes in biological processes, horizontal advection, and diffusion may also contribute to the nutrient changes and are represented as the residual between the total nutrient changes, $\Delta\mathcal{N}$, and $\Delta\mathcal{N}_h$.

Ocean-biogeochemical model setup

We carry out a suite of ocean-biogeochemical simulations to compare the role of wind and surface buoyancy forcing in global nutrient redistribution. The ocean component is the Massachusetts Institute of Technology General Circulation Model (MITgcm) with a nonlinear equation of state[45]. The model resolution is 1° in longitude and 0.5° in latitude. The model domain is similar to CESM2 but without the Arctic to avoid the singularity problem in the polar region. In the vertical, there are 30 layers ranging from 10 m at the top to 369 m at the bottom. Vertical mixing is handled by the K-Profile parameterization[46]. Unresolved eddies are represented using the skew-flux form of the Gent–McWilliams parameterization with a background diffusivity of 1,000 $m^2\,s^{-1}$. Isopycnal diffusion due to eddies is parameterized using the Redi scheme with a diffusivity of 1,000 $m^2\,s^{-1}$. The model is forced with surface forcing taken from CESM2. Temperature at the surface is restored to monthly sea surface temperature with a relaxation timescale of 14 days[47] and a net surface heat flux. Surface salinity is forced by monthly surface freshwater flux, which includes precipitation, evaporation, ice melt, and river runoff. A weak relaxation of the surface salinity to CESM2 piControl climatology is also included to avoid possible bi-stability of the overturning circulation due to the mixed boundary conditions[48].

The biogeochemistry component is a modified version of Biogeochemistry with Light, Iron, Nutrients, and Gas (BLING)[49,50] to include the silicon cycle. The original BLING model includes an implicit physiological model of growth co-limitation by light, temperature, phosphate, and iron and an implicit ecological model of partitioning into remineralized and dissolved pools. It solves for dissolved inorganic phosphate, dissolved inorganic carbon, dissolved organic phosphate, alkalinity, oxygen, and dissolved iron. The modifications to BLING include an added phytoplankton group, diatoms, and silicon cycle, largely following a more sophisticated biogeochemical model, TOPAZv2[51]. We force the biogeochemistry model with climatological monthly iron fluxes, surface wind speed, and sea ice coverage from CESM2 piControl, which are kept constant throughout the suite of different simulations.

A total of four experiments were carried out using the ocean-biogeochemical model: "Control", "Wind", "Buoyancy", and "4×CO_2". In "Control", both surface wind and buoyancy forcing (surface heat flux, surface temperature, surface freshwater flux, and surface salinity) are taken from CESM2 piControl. "Control" is run for over 4,000 years to achieve an approximately steady state. The other three experiments were initialized from the end of "Control" and continued for 300 years. In "Wind", the surface wind is taken from CESM2 4×CO_2 (monthly climatology over years 150–200) but surface buoyancy forcing is kept the same as in "Control". In "Buoyancy", the surface wind is kept the same as in "Control" but surface buoyancy forcing is taken from CESM2 4×CO_2 (monthly climatology over years 150–200). In "4×CO_2", both surface wind and buoyancy forcing are taken from CESM2 4×CO_2 (monthly climatology over years 150–200). "Control" largely reproduces the structure of the nutrients in CESM2 (Supplementary Fig. 12). With surface forcing from CESM2 4×CO_2, "4×CO_2" also approximately reproduces the global nutrients reorganization (Supplementary Fig. 12). Comparison of "Wind" and "Buoyancy" with "Control", quantified as their differences averaged over years 250–300 after perturbations, shows the impacts of changes in surface wind and surface buoyancy forcing, respectively, on the overturning responses and nutrients reorganization.

Data availability

The CESM2 model output was downloaded from the Earth System Grid Federation node (https://esgf-node.llnl.gov/search/cmip6/). The climatological Si data used in creating Fig. 1 were downloaded from GLODAPv2 (https://glodap.info/). Source data for Figs. 2–4 are provided in this paper. Model outputs from the MITgcm experiments are made publicly available from the online open access repository, Figshare, with https://doi.org/10.6084/m9.figshare.26787751. Source data are provided in this paper.

Code availability

The code for reproducing the ocean-biogeochemical experiments in this study is made publicly available from the online open-access repository, Figshare, with https://doi.org/10.6084/m9.figshare.26129629.

References

1. Bopp, L. et al. Multiple stressors of ocean ecosystems in the 21st century: projections with CMIP5 models. *Biogeosciences* **10**, 6225–6245 (2013).
2. Moore, J. K. et al. Sustained climate warming drives declining marine biological productivity. *Science* **359**, 1139–1143 (2018).
3. Kwiatkowski, L. et al. Twenty-first century ocean warming, acidification, deoxygenation, and upper-ocean nutrient and primary production decline from CMIP6 model projections. *Biogeosciences* **17**, 3439–3470 (2020).
4. Held, I. M. et al. Probing the fast and slow components of global warming by returning abruptly to preindustrial forcing. *J. Clim.* **23**, 2418–2427 (2010).
5. Long, S.-M., Xie, S.-P., Zheng, X.-T. & Liu, Q. Fast and slow responses to global warming: sea surface temperature and precipitation patterns. *J. Clim.* **27**, 285–299 (2014).
6. Liu, Y., Moore, J. K., Primeau, F. & Wang, W. L. Reduced CO_2 uptake and growing nutrient sequestration from slowing overturning circulation. *Nat. Clim. Change*. https://doi.org/10.1038/s41558-022-01555-7 (2022).
7. Yin, J. H. A consistent poleward shift of the storm tracks in simulations of 21st-century climate. *Geophys. Res. Lett.* **32**, L18701 (2005).
8. Goyal, R., Sen Gupta, A., Jucker, M. & England, M. H. Historical and projected changes in the southern hemisphere surface westerlies. *Geophys. Res. Lett.* **48**, e2020GL090849 (2021).
9. Sarmiento, J. L., Gruber, N., Brzezinski, M. & Dunne, J. High-latitude controls of thermocline nutrients and low-latitude biological productivity. *Nature* **427**, 56–60 (2004).
10. Anderson, R. F. et al. Wind-driven upwelling in the southern ocean and the deglacial rise in atmospheric CO_2. *Science* **323**, 1443–1448 (2009).
11. Dumont, M. et al. The nature of deep overturning and reconfigurations of the silicon cycle across the last deglaciation. *Nat. Commun.* **11**, 1–11 (2020).
12. Dansgaard, W. et al. North Atlantic climatic oscillations revealed by deep Greenland ice cores. *Clim. Process. Clim. Sensit.* **29**, 288–298 (1984).
13. Menviel, L., Skinner, L. C., Tarasov, L. & Tzedakis, P. C. An ice–climate oscillatory framework for Dansgaard–Oeschger cycles. *Nat. Rev. Earth Environ.* **1**, 677–693 (2020).
14. Sigman, D. M., Hain, M. P. & Haug, G. H. The polar ocean and glacial cycles in atmospheric CO_2 concentration. *Nature* **466**, 47–55 (2010).
15. Toggweiler, J. & Samuels, B. Effect of Drake passage on the global thermohaline circulation. *Deep Sea Res. I* **42**, 477–500 (1995).
16. Toggweiler, J., Russell, J. L. & Carson, S. R. Midlatitude westerlies, atmospheric CO_2, and climate change during the ice ages. *Paleoceanogr.* https://doi.org/10.1029/2005PA001154 (2006).
17. Abernathey, R., Marshall, J. & Ferreira, D. The dependence of Southern Ocean meridional overturning on wind stress. *J. Phys. Oceanogr.* **41**, 2261–2278 (2011).
18. Dufour, C. O. et al. Standing and transient eddies in the response of the Southern Ocean meridional overturning to the southern annular mode. *J. Clim.* **25**, 6958–6974 (2012).

19. Meredith, M. P., Naveira Garabato, A. C., Hogg, A. M. & Farneti, R. Sensitivity of the overturning circulation in the Southern Ocean to decadal changes in wind forcing. *J. Clim.* **25**, 99–110 (2012).
20. Bishop, S. P. et al. Southern ocean overturning compensation in an Eddy-resolving climate simulation. *J. Phys. Oceanogr.* **46**, 1575–1592 (2016).
21. Cheng, W., Chiang, J. C. & Zhang, D. Atlantic meridional overturning circulation (AMOC) in CMIP5 models: RCP and historical simulations. *J. Clim.* **26**, 7187–7197 (2013).
22. Weijer, W., Cheng, W., Garuba, O., Hu, A. & Nadiga, B. CMIP6 models predict significant 21st century decline of the Atlantic Meridional Overturning Circulation. *Geophys. Res. Lett.* **47**, e2019GL086075 (2020).
23. Sun, S., Thompson, A. F. & Eisenman, I. Transient overturning compensation between Atlantic and Indo-Pacific basins. *J. Phys. Oceanogr.* **50**, 2151–2172 (2020).
24. Sun, S. & Thompson, A. F. Centennial changes in the Indonesian throughflow connected to the Atlantic Meridional overturning circulation: the ocean's transient conveyor belt. *Geophys. Res. Lett.* **47**, e2020GL090615 (2020).
25. Sun, S., Thompson, A. F., Xie, S.-P. & Long, S.-M. Indo-Pacific warming induced by a weakening of the Atlantic meridional overturning circulation. *J. Clim.* **35**, 815–832 (2022).
26. Saenko, O. A., Schmittner, A. & Weaver, A. J. The Atlantic–Pacific seesaw. *J. Clim.* **17**, 2033–2038 (2004).
27. Okazaki, Y. et al. Deepwater formation in the North Pacific during the last glacial termination. *Science* **329**, 200–204 (2010).
28. Chikamoto, M. O. et al. Variability in North Pacific intermediate and deep water ventilation during Heinrich events in two coupled climate models. *Deep Sea Res. II* **61**, 114–126 (2012).
29. Menviel, L., England, M. H., Meissner, K., Mouchet, A. & Yu, J. Atlantic–Pacific seesaw and its role in outgassing CO_2 during Heinrich events. *Paleoceanogr.* **29**, 58–70 (2014).
30. Eyring, V. et al. Overview of the coupled model intercomparison project phase 6 (CMIP6) experimental design and organization. *Geosci. Model Dev.* **9**, 1937–1958 (2016).
31. Sarmiento, J. L. & Gruber, N. *Ocean Biogeochemical Dynamics* (Princeton University Press, 2006).
32. Menviel, L. et al. Southern Hemisphere westerlies as a driver of the early deglacial atmospheric CO_2 rise. *Nat. Commun.* **9**, 2503 (2018).
33. Swart, N. C., Gille, S. T., Fyfe, J. C. & Gillett, N. P. Recent southern ocean warming and freshening driven by greenhouse gas emissions and ozone depletion. *Nat. Geosci.* **11**, 836 (2018).
34. Schmittner, A. Decline of the marine ecosystem caused by a reduction in the Atlantic overturning circulation. *Nature* **434**, 628–633 (2005).
35. Schmittner, A. & Galbraith, E. D. Glacial greenhouse-gas fluctuations controlled by ocean circulation changes. *Nature* **456**, 373–376 (2008).
36. Nielsen, S. B., Jochum, M., Pedro, J. B., Eden, C. & Nuterman, R. Two-timescale carbon cycle response to an AMOC collapse. *Paleoceanogr. Paleoclimatol.* **34**, 511–523 (2019).
37. Stewart, J. A. et al. Arctic and Antarctic forcing of ocean interior warming during the last deglaciation. *Sci. Rep.* **13**, 22410 (2023).
38. Sigman, D. M. et al. The Southern Ocean during the Ice Ages: a review of the Antarctic surface isolation hypothesis, with comparison to the North Pacific. *Quat. Sci. Rev.* **254**, 106732 (2020).
39. Ito, T. & Follows, M. J. Preformed phosphate, soft tissue pump and atmospheric CO_2. *J. Mar. Res.* **63**, 813–839 (2005).
40. Danabasoglu, G. et al. The community earth system model version 2 (CESM2). *J. Adv. Model. Earth Syst.* **12**, e2019MS001916 (2020).
41. Heuzé, C., Heywood, K. J., Stevens, D. P. & Ridley, J. K. Southern Ocean bottom water characteristics in CMIP5 models. *Geophys. Res. Lett.* **40**, 1409–1414 (2013).
42. Martin, J. H., Fitzwater, S. E. & Gordon, R. M. Iron deficiency limits phytoplankton growth in Antarctic waters. *Glob. Biogeochem. Cycles* **4**, 5–12 (1990).
43. Hauck, J. et al. On the Southern Ocean CO_2 uptake and the role of the biological carbon pump in the 21st century. *Global Biogeochem. Cycle* **29**, 1451–1470 (2015).
44. Talley, L. D. Closure of the global overturning circulation through the Indian, Pacific, and Southern Oceans: schematics and transports. *Oceanography* **26**, 80–97 (2013).
45. Jackett, D. R. & Mcdougall, T. J. Minimal adjustment of hydrographic profiles to achieve static stability. *J. Atmos. Ocean. Technol.* **12**, 381–389 (1995).
46. Large, W. G., McWilliams, J. C. & Doney, S. C. Oceanic vertical mixing: a review and a model with a nonlocal boundary layer parameterization. *Rev. Geophys.* **32**, 363–403 (1994).
47. Haney, R. L. Surface thermal boundary condition for ocean circulation models. *J. Phys. Oceanogr.* **1**, 241–248 (1971).
48. Stommel, H. Thermohaline convection with two stable regimes of flow. *Tellus* **13**, 224–230 (1961).
49. Dunne, J. P. et al. Simple global ocean biogeochemistry with light, iron, nutrients and gas version 2 (BLINGv2): model description and simulation characteristics in GFDL's CM4. 0. *J. Adv. Model. Earth Syst.* **12**, e2019MS002008 (2020).
50. Verdy, A. & Mazloff, M. R. A data assimilating model for estimating Southern Ocean biogeochemistry. *J. Geophys. Res. Oceans* **122**, 6968–6988 (2017).
51. Dunne, J. P. et al. GFDL's ESM2 global coupled climate-carbon earth system models. Part I: Physical formulation and baseline simulation characteristics. *J. Clim.* **25**, 6646–6665 (2012).
52. Olsen, A. et al. The Global Ocean Data Analysis Project version 2 (GLODAPv2)—an internally consistent data product for the world ocean. *Earth Syst. Sci. Data* **8**, 297–323 (2016).

Acknowledgements

Without implying their endorsement, we are grateful for helpful discussions with Daniel Sigman, Jess Adkins, Keith Moore, Frankie Pavia, and Ariane Verdy. J.Y. acknowledges support from NSF China (42330403, 42076056). A.F.T. was supported by NSF OCE-2023259, the Resnick Sustainability Institute, and the David and Lucille Packard Foundation.

Author contributions

S.S. and A.F.T. conceived the study. S.S. carried out the model simulations and analyzed the model output. S.S. and A.F.T. drafted the manuscript. J.Y. and L.W. contributed to discussions and improving the manuscript.

Competing interests

The authors declare no competing interests.

Additional information

Supplementary information The online version contains supplementary material available at https://doi.org/10.1038/s41467-024-52200-0.

Correspondence and requests for materials should be addressed to Shantong Sun.

Peer review information *Nature Communications* thanks the anonymous reviewers for their contribution to the peer review of this work. A peer review file is available.